Projection of Sea Ice Conditions in Nunatsiavut (Labrador)

Thomas Amo Kyeimiah,

Department of Atmospheric and Oceanic Sciences

McGill University, Montreal

AUGUST, 2024

A thesis submitted to McGill University in partial fulfillment of the requirements of the degree of

Master of Atmospheric and Oceanic Sciences

Supervisor: Professor Bruno Tremblay

Abstract

Of all sub-regions of the Canadian Arctic, the Labrador and Baffin Bay display the largest negative trend in summer sea ice area, raising important, questions regarding the length of the “usable-sea-ice season” for coastal communities of Nunatsiavut. In this work, we focus on projected changes in sea ice thickness and extent in the Labrador Sea and Baffin Bay, and more specifically on changes in sea ice season length for four coastal communities, namely Nain, Hopedale, Postville and Rigolet using output diagnostics from the High-Resolution (0.1 degree) Community Earth System Model version 1.3 (CESM1.3-HR) for the period 1850-2100. Given that this high-resolution model does not resolve landfast ice nor the fjord in which the coastal communities are located, the sea ice season length is derived from surface air temperature data (resolved by the model) and a simple freezing degree day model, validated using in-situ, reanalysis and remote sensing data. Results for the Baffin Bay and Labrador Sea show a remarkably stable maximum march sea ice extent in the Labrador Sea followed by a rapid transition to winter ice-free conditions around 2060 when the Arctic Ocean becomes seasonally ice-free and no longer advect thick multi-year sea ice south through the Nares Strait and along the Labrador coastline. This is in contrast with the lower resolution CESM2-LE showing a re-expansion of the maximum sea ice extent starting in the middle of the 21st century followed by a sudden collapse at the end of the century due to a restratification of Labrador Sea and shutdown

of deep convection. These results show the importance of resolving small scale process for regional climate projection. Also of interest is the gradual decline in the “usable-sea-ice” season and sporadic extremely large inter-annual variation in sea ice season length in the mid 21st century - a signal that is robust to model spatial resolution and presence or absence of deep convection in the Labrador Sea.

Abrégé

De toutes les sous-régions de l'Arctique canadien, le Labrador et la baie de Baffin présentent la tendance la plus marquée en termes de déclin de superficie de glace de mer estivale, soulevant d'importantes questions concernant la durée d'une "saison de glace de mer utilisable" pour les communautés côtières du Nunatsiavut. Ce projet se concentre sur les changements projetés dans l'épaisseur et l'étendue de glace de mer dans la mer du Labrador et la baie de Baffin et plus particulièrement sur la durée de la saison de glace de mer pour quatre communautés côtières, soit Nain, Hopedale, Postville et Rigolet. Nous utilisons des variables diagnostiques du Community Earth System Model version 1.3 (CESM1.3-HR) à haute-résolution (0,1 degré) s'étendant sur la période 1850-2100. Puisque ce modèle à haute-résolution ne résout pas la glace côtière (landfast ice), ni le fjord dans lequel sont établies les communautés côtières, la durée de la saison de glace de mer est calculée à partir des données de température de l'air en surface (résolue par le modèle) et d'un modèle simple de degrés-jours de gel, et validée à partir de données in situ, de réanalyse et de télédétection. Les résultats montrent une étendue maximale de glace de mer remarquablement stable dans la mer du Labrador, suivie d'une transition rapide vers des conditions hivernales sans glace vers 2060 lorsque l'océan Arctique devient libre de glace en été et ne transporte plus de glace épaisses vers le sud à travers le détroit de Nares et le long de la côte du Labrador. Ceci contraste avec les résultats du modèle à plus basse

résolution CESM2-LE, qui montrent une réexpansion de l'étendue maximale de glace de mer à partir du milieu 21e siècle, suivie d'une réduction drastique et soudaine à la fin du siècle due à une restratification de la mer du Labrador et d'un arrêt de la convection profonde. Ces résultats soulignent l'importance de résoudre les processus à petite échelle pour une meilleure projection climatique régionale. Également d'intérêt sont le déclin progressif de la durée d'une “saison de glace de mer utilisable” et la très grande variation interannuelle qui apparaît sporadiquement dans la durée de la saison de glace de mer au milieu du 21e siècle - un signal robuste à la résolution spatiale du modèle et à la présence ou absence de convection profonde dans la mer du Labrador.

Acknowledgements

First and foremost, I am deeply indebted to the support provided by the Grant and Contribution from the Canadian Ice Service awarded to Tremblay. This project is also a contribution to a Natural Science and Engineering Research Council (NSERC) Discovery Grant and a NASA ROSE grant (Grant 80NSSC20K1259), both awarded to Tremblay. Thanks to Jaison Kurian from Texas A&M University for the CESM1.3-HR and CESM1.3-LR data, and to Joey Angnatok and the Nunatsiavut Research Center for their observed data.

I would like to express my deepest gratitude to my supervisor, Professor Bruno Tremblay, for his invaluable guidance and support throughout my research journey. I am also profoundly grateful to Adrienne Tivy, Jean-François Lemieux, and Mathieu Plante for their thoughtful contributions and time in reviewing my work.

A special thank you goes to the Department of Atmospheric and Oceanic Sciences at McGill University for providing an enriching academic environment. I would like to extend my heartfelt thanks to my colleagues and friends, whose camaraderie and assistance have been a source of motivation and inspiration. Their support has been invaluable, both professionally and personally.

To my mom, Hannah Okwan, and my elder sister, Perpetual Okwan, thank you for your unwavering prayers, love, and encouragement. Lastly, I am grateful to everyone who contributed to this thesis. Your support and encouragement have been a cornerstone of my success.

Data Availabilty

The model output (CESM1.3-HR) used in this work is publicly available from the iHESP data archive portal (https://ihesp.github.io/archive/products/ds_archive/Sunway_Runs.html) and documented in Chang et al. (2020). The CESM2-LE data is available on the NSF National Center for Atmospheric Research platform (https://www.earthsystemgrid.org/dataset/ucar.cgd.cesm2le.output.html). The CIS gridded version of ice charts is not public but can be made available to the community upon request. The observed Nain data can also be made publicly available to the community upon request. The NSIDC-CDR SIC (https://noaadata.apps.nsidc.org/NOAA/G02202_V4/north/) and ERA5 reanalysis data (https://www.ecmwf.int/en/forecasts/datasets/reanalysis-datasets/era5) are available online. All scripts used to obtain results are publicly available at All scripts used to obtain results are publicly available at https://github.com/devThom-studios/Sea-Ice-Projection-Nunatsiavut.

Table of Contents

List of Figures

List of Abbreviations

Acronym	Definition
CAM5	Community Atmosphere Model version 5.
CICE4	Community Ice Code version 4.
CIS	Canadian Ice Service.
CISDA	Canadian Ice Service Digital Archive.
CLM4	Community Land Model version 4.
CMIP6	Coupled Model Intercomparison Project Phase 6.
DMSP	Defense Meteorological Satellite Program.
EA	Eastern Arctic.
EC	East Coast.
ECMWF	European Centre for Medium-Range Weather Forecasts.
EASE	Equal-Area Scalable Earth.
ERA5	Fifth generation ECMWF atmospheric reanalysis of the global climate.
FDD	Freezing Degree Days.
GIS	Geographic Information System.
GtCO_2	Gigatonnes of Carbon Dioxide.
HB	Hudson Bay.
JCOMM	Joint Technical Commission for Oceanography and Marine Meteorology.
MODIS	Moderate Resolution Imaging Spectroradiometer.
MOAR	Mother Of All Runs.
NAO	North Atlantic Oscillation.
NASA	National Aeronautics and Space Administration.
NSIDC-CDR	National Snow and Ice Data Center - Climate Data Record.
POP2	Parallel Ocean Program version 2.
RADARSAT	Canadian Remote Sensing Satellite Series
SIC	Sea Ice Concentration.
SIE	Sea Ice Extent.
SIGRID	Sea Ice GeoReferenced Information and Data.
SIT	Sea Ice Thickness.
SMMR	Scanning Multichannel Microwave Radiometer.

SSM/I	Special Sensor Microwave/Imager.
SSMIS	Special Sensor Microwave Imager/Sounder.
SSP	Shared Socioeconomic Pathway.
SSS	Sea Surface Salinity.
WMO	World Meteorological Organization.

Chapter 1

INTRODUCTION

The Arctic is projected to become seasonally ice-free before the middle of the century, with anthropogenic CO_2 emissions less than 1000 GtCO_2 above the 2019 level, in the majority of climate models and across all scenarios (Notz and Community, 2020). In the eastern Canadian sub-Arctic, significant warming in Labrador has been observed, with an annual mean, winter and summer temperature increase of approximately 1.5°C, 2.0°C and 1.0°C over the period from 1881 to 2011 (Ouellet-Bernier et al., 2021a). Of the six largest rate of sea ice decline report by the Canadian Ice Service in the Canadian sub-Arctic for the period 1968-2010, two are located on the Canadian east coast: in the Northern Labrador Sea (17% per decade) and Baffin Bay (10%) (Statistics Canada, 2012). These changes are affecting communities in the Arctic and subarctic regions that rely on the natural environment for subsistence and recreational activities(Felt et al., 2012; ACIA, 2004; Nickels et al., 2005).

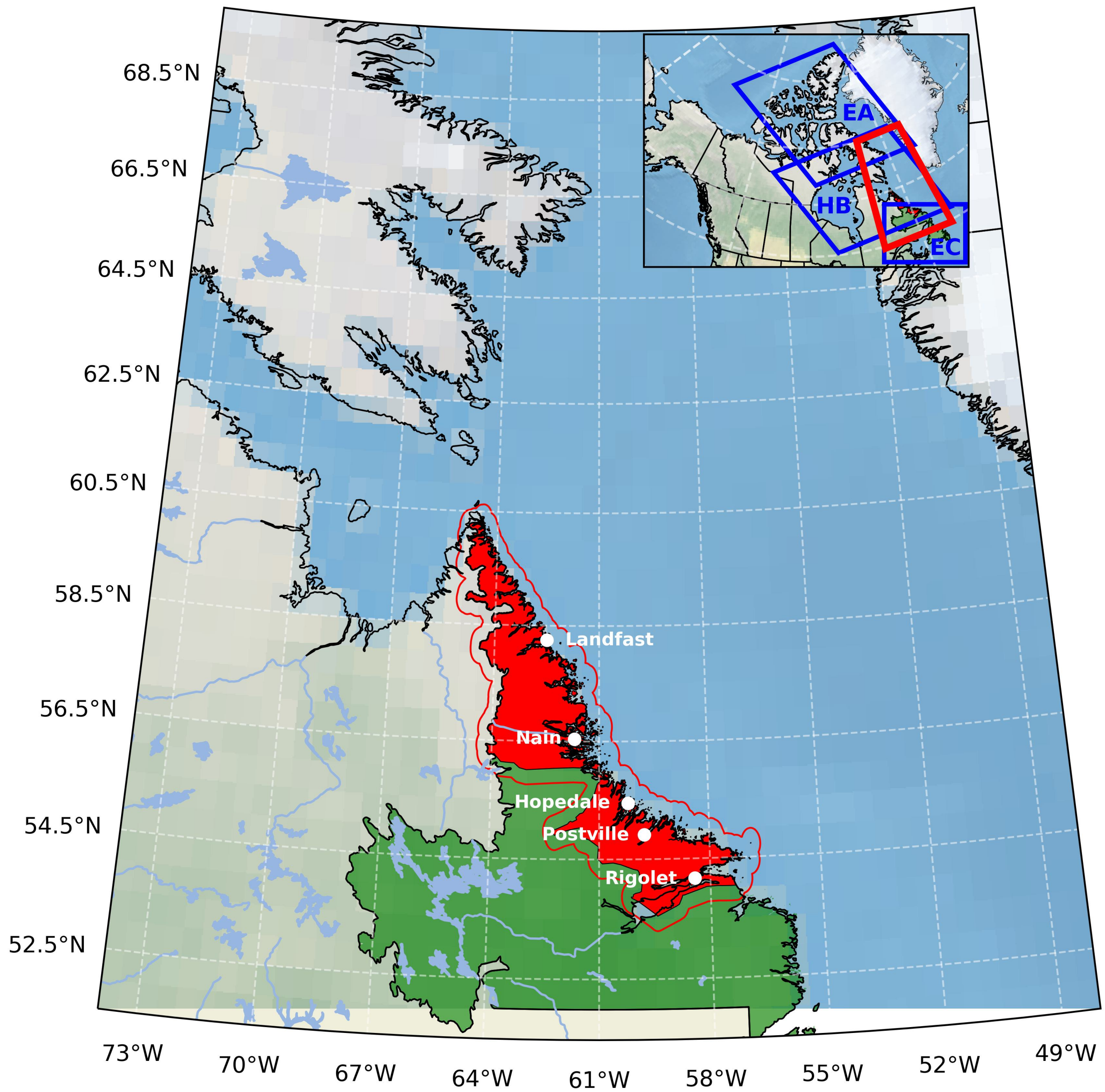

Figure 1.1: Map of Nunatsiavut (Labrador, shaded red), locations of key coastal communities and selected grid cells for the landfast analysis (white dots). Inset shows the study area within the broader Canadian Arctic Archipelago, from the Canadian Ice Service covering the domain: Eastern Arctic (EA), Hudson Bay (HB), and East Coast (EC) (blue rectangular box).

Nunatsiavut, meaning 'our beautiful land' in the Inuktitut language, includes a significant portion of the Labrador coast (Cunsolo et al., 2017). This area is rich in cultural heritage and biodiversity and one of the Inuit regions where residents have identified changes that are affecting their well-being (Felt et al., 2012; Cunsolo et al., 2017; CBC News, 2021; Newswire, 2021). For the Nunatsiavut Inuit, sea ice dictates the rhythms of life, and is essential to the socio-ecological system of Nunatsiavut and is considered an extension of the land, making it crucial for cultural activities, communication, mobility, and livelihood (Cuerrier et al., 2015; Ouellet-Bernier et al., 2021b; Gearheard et al., 2006; Pearce et al., 2009). Sea ice serves not only as a symbol of heritage but also as a conduit for community connection and a barometer for change.

Sea ice in Baffin Bay and Labrador Sea first appear on the Canadian eastern sub arctic in November and disappear in august primarily formed locally through thermodynamic processes with some advection from the Arctic Ocean through the Nares Strait drifting southward along the Labrador coast. The sea ice cover is assymmetric from west to east with cold fresher water from the Canadian Arctic Archipelago and the Arctic flowing southward along the Labrador Coast promoting local sea ice formation and some advection of thick multi-year ice from the Arctic through Narest Strait (Kwok, 2005; Münchow, 2016; Howell et al., 2023), and relatively warmer water of Atlantic origin flowing northward and keeping the south-west coast of Greenland mainly ice free (Close et al., 2018; Weijer et al., 2021). Of particular interest is the ice-free conditions and deep water formation at the center of Labrador Sea where cold salty waters convects to different depth depending mainly on the salinity of the surface waters (Yashayaev et al., 2007; Yashayaev, 2024). Results form a regional coupled ice-ocean model with specified atmospheric forcing project an increase in sea surface and bottom temperatures, a decrease in salinity, and a reduced winter sea ice extent of 70% over the Labrador and Newfoundland shelves from 2040 to 2069 compared to the 1981 to 2010 period (Han et al., 2019).

Factor influencing the extent of sea ice and surface salinity of surface waters in the Labrador Sea include synoptic and mesoscale storms, themselves dependent on the state of the North Atlantic Oscillation, that advects sea ice offshore in region of saltier waters (Häkkinen, 2002; Wu et al., 2023; Vaideanu et al., 2023). The NAO also affects sea ice on the eastern Canadian coast on longer time scale (interannual and decadal) with anomalous southern advection of warm air on the northeast North Atlantic and northern advection of colder air in the Baffin Bay Labrador Sea region (Deser et al., 2002, 2004; Eden and Willebrand, 2001). These sources of natural variability are superimposed on a greenhouse-induced warming signal disentangling the natural from the forced variability in this region affected by a larger number of small scale process and located near the center of action of the NAO remains a challenge.

In this work, we focus on projections of sea ice conditions – chiefly the length of the ice season and mechanism changes – in Nunatsiavut from the high-resolution Community Earth System Model (CESM1.3-HR) together with in-situ ice thickness observations from local communities and satellite images from the from the Canadian Ice Service (CIS) and Climate data records (CDR). The results from lower resolution version of the same model are also discussed to assess the robustness of the results from th high resolution model.

The paper is organized as follows. Chapter 2 describes the model diagnostics from the High- and Low-Resolution Community Earth System Model (CESM1.3-HR, CESM1.3-LR), Large Ensemble of Community Earth System Model version 2 (CESM2-LE), in-situ observations from Nain and satellite data from the Canadian Ice Service. Chapter 3 describes the method used to calculate the sea ice extent and length of the ice season for specific coastal communities at the regional scales. The results and discussion are presented in Chapter 4. The main conclusions and future work are summarize in Chapter 5.

Chapter 2

DATA

2.1 Sea Ice Concentration: Canadian Ice Service (CIS)

We use the Canadian Ice Service (CIS) regional ice chart database (CISDA; CIS Digital Archive) for the Eastern Arctic (EA), Hudson Bay (HB), and East Coast (EC) at monthly temporal resolution during winter and weekly resolution during summer prior to 2005; and weekly resolution all years thereafter (see Figure 1.1). CISDA is a collection of regional ice charts produced by ice analysts from low and high resolutions satellite products (SSM/I sensors, MODIS, RADARSAT-1), aerial observation, ship reports, and operational models (Galley et al., 2012; Pizzolato et al., 2014; Tivy et al., 2011). The digital ice charts contain ice concentraion, ice thickness and floe size for polygons of different ice types (e.g., land-fast ice, first-year ice, multi-year ice, deformed ice, pack ice, Nilas ice) using the World Meteorological Organization's (WMO) Egg code. The data are stored using the ArcInfo Geographical Information System (GIS); the raw data are gridded using nearest-point interpolation on a 10 x 10 km EASE grid from 1990 to December 2020 following the Sea Ice GeoReferenced Information and Data (SIGRID) standard guidelines (JCOMM, 2004; Galley et al., 2012; Agnew and Howell, 2003). Note that the land masks changes between ice charts and the data is stored on the most extensive landmark for consistency.

2.2 Sea Ice Concentration and Thickness: High- and Low-Resolution Community Earth System Model (CESM1.3-HR, CESM1.3-LR) and Low-Resolution Community Earth System Model

We use the sea ice concentration, thickness, and 2m temperature diagnostics from the International Laboratory for High-Resolution Earth System Prediction (iHESP), produced using both high-resolution and low-resolution configurations of the Community Earth System Model (Version 1.3, Meehl et al. 2019). iHESP is a collaborative effort involving Texas A&M University, the National Center for Atmospheric Research (NCAR), and the Qingdao Pilot National Laboratory for Marine Science and Technology (Chang et al., 2020). CESM1.3-HR includes fourcomponents: the Community Atmosphere Model version 5 (CAM5, Neale et al. 2010; Chang et al. 2020), the Parallel Ocean Program version 2 Danabasoglu et al. 2012; Smith et al. 2010; Small et al. 2014; Chang et al. 2020), the Community Ice CodE version 4 Hunke et al. 2010; Bailey et al. 2011; Small et al. 2014; Chang et al. 2020), and the Community Land Model version 4 Lawrence et al. 2011; Small et al. 2014; Chang et al. 2020). The atmosphere and land component share the same grid with a nominal horizontal resolution of $0.25°$; the atmosphere model has 30 vertical levels with a model top at 3 hPa (Chang et al., 2020). The ocean and sea-ice models are discretized using a B-grid on a tripolar grid, with a nominal resolution of $0.1°$; two poles located over northern Canada and Russia to avoid the singularity at the North Pole, and a regular spherical polar grid in the Southern Hemisphere. POP2 has 62 vertical levels with a 10 m resolution in the first 155 m, gradually coarsening to 250 m near the maximum depth of 6000 m (Chang et al., 2020; Meehl et al., 2019; Zhang et al., 2020). The ocean model has a 3rd order upwind advection scheme, a K-profile vertical mixing parameterization (Large et al., 1994), and explicitely resolves eddy-induced vertical transport. The sea ice component of the model includes the elastic-viscous plastic rheology (Hunke and Dukowicz, 2002), a subgrid scale ice thickness distribution with multiple levels in each category (Bitz et al., 2001; Lipscomb, 2001), and an energy-conserving thermodynamic scheme that accounts for the effect of internal brine pockets (Bitz and Lipscomb, 1999).

CESM1.3-HR has 10 ensemble members with one ensemble member covering the period from 1850 to 2100, and nine ensemble members covering the period from 1920 to 2100. The simulations were initialized from a 500-year pre-industrial control simulation. The model was forced with historical data for the period 1850 or 1920 until 2005 and with greenhouse gas from the Representative Concentration Pathway 8.5 from 2006-2100 (Chang et al., 2020). As of today, monthly diagnostic outputs are available for three of the ten ensemble members from 1920 to 2100. More details about CESM1.3-HR can be found in Chang et al. (2020).

2.3 Sea Ice Concentration: Community Earth System Model version 2 - Large Ensemble (CESM2-LE)

We use the sea ice concentration from Community Earth System Model Large Ensemble version 2 (CESM2-LE). The CESM2-LE consists of 100 large ensemble members at 1° spatial resolution covering the period 1850-2100 under CMIP6 historical and SSP370 future radiative forcing scenarios (Eyring et al., 2016; Rodgers et al., 2021), which is composed of seven geophysical model components and an additional component for external system processing (CESM2, 2020). The sea ice component is the Community Ice CodE version 5 (CICE5, Muntjewerf et al. 2021; Hunke et al. 2017). CICE5 uses a third-order advection scheme and elastic viscous-plastic rheology (Hunke and Dukowicz, 2002). The temperature and salinity vertical profiles of sea ice are resolved in eight vertical layers for each category of ice thickness and three snow layer (Muntjewerf et al., 2021). The model was initialized using a combination of macro and micro perturbations. Macro perturbations were implemented using 20 independent restart files at 10-year intervals from 1001–1191, from the preindustrial control simulation without explicit perturbations. The first ten members of the control simulation were chosen to minimize drift, while the last ten members include the extensive Mother Of All Runs (MOAR) output. Twenty micro-perturbations are applied to each of the years 1231, 1251, 1281, and 1301 of the preindustrial simulation, using small random perturbations $10^{-14}K$ applied to the atmospheric temperature field for total of 80 micro-perturbation runs. The first half of the 100 members were subjected to the standard CMIP6 biomass-burning emissions. The other half used a temporally smoothed biomass burning emission inventory, achieved by implementing an 11-year running mean filter from 1990 to 2020 (Heyblom et al., 2022; Rodgers et al., 2021; Van Marle et al., 2017; CESM2-LE, 2023). Temporal smoothing of the biomass burning emissions was implemented at each grid point after regridding them to the CESM2 grid. The objective of the smoothed forcing was to preserve the total emissions as closely as possible while mitigating the significant fluctuations in interannual variability (Rodgers et al., 2021).

2.4 Sea Ice Concentration: Climate Data Records

We use the monthly sea ice concentration (SIC) data from the National Snow and Ice Data Center (NSIDC) Climate Data Record (CDR, version 4). CDR-SIC is derived from the Scanning Multichannel Microwave Radiometer (SMMR), the Special Sensor Microwave/Imager (SSM/I), and the Special Sensor Microwave Imager/Sounder (SSMIS), flying on the Defense Meteorological Satellite Program (DMSP) satellites 5D-2/F11, 5D-2/F13, 5D-2/F8, 5D-3/F17, and the Nimbus-7 satellites. The data is stored on a 25 x 25 km polar stereographic grid centered on the North Pole from 25 October 1978 to today for both the Arctic and Southern Oceans (Meier et al., 2021). The sea ice concentration products are based on the NASA Team and Bootstrap algorithms. The NASA Team algorithm compares brightness temperature (Tb) ratios from channels with horizontal (H) and vertical (V) polarization (19V, 19H, 37V) to identify surface types, using fixed tie-points and a weather filter (Cavalieri et al., 1984, 1997) while the Bootstrap algorithm uses Tb from 37H, 37V, and 19V channels, with dynamic tie points (Comiso, 1986, 1995; Comiso and Nishio, 2008). Both algorithms have limitations, including reduced accuracy in regions with surface melt or thin ice, and in the marginal ice zone, where ice thermodynamic processes are key to changing sea ice condition (Kern et al., 2020; Comiso, 2023; Agnew and Howell, 2003).

2.5 2m Air Temperature: ERA5

We use the 2m air temperature data from the ERA5 reanalysis, the fifth-generation dataset from the European Centre for Medium-Range Weather Forecasts (ECMWF) for global climate and weather over the past eight decades. Available from 1940 onwards, ERA5 replaces the ERA-Interim reanalysis (Hersbach et al., 2023). Significant improvements over

ERA-Interim include better availability and higher temporal resolution (hourly) (Urraca et al., 2018; Yu et al., 2021; Hersbach et al., 2023). ERA5 combines a global climate model (representing physical processes and energy fluxes in the Earth's atmosphere, oceans, and land surfaces) with in situ and satellite observations, known as data assimilation (Urban et al., 2021; Hersbach et al., 2023). ERA5 data is gridded on a regular latitude-longitude grid of 0.25 degrees for reanalysis and 0.5 degrees for uncertainty estimates (0.5 and 1 degree respectively for ocean waves) and 137 hybrid signal pressure levels in the vertical (Urban et al., 2021; Hersbach et al., 2023). ERA5 benefits from numerous advancements in observation operators and a decade of developments in model physics, core dynamics, and data assimilation (Olauson, 2018; Zhu et al., 2021; Hersbach et al., 2023). The 2m temperature represents the air temperature at 2m above the surface of land, sea, or inland waters. It is calculated by interpolating between the lowest model level and the Earth's surface, taking into account atmospheric conditions (Hersbach et al., 2023).

2.6 Sea ice thickness: Nunatsiavut Research Center (Nain)

We use the observed ice thickness and snow depth data from the Nunatsiavut Research Center in Nain. The dataset spans the years 2009 to 2023, with the two years missing (2012 and 2014). The ice thickness is measured using a heated cable following the protocol established by Mahoney et al. (2009). Snow depth was measured in a 10 m x 10 m area using snow stakes.

Chapter 3

METHODOLOGY

3.1 Sea Ice Extent (SIE)

The Sea ice extent (SIE) is calculated as the sum of all grid cell areas with at least 15% SIC in a given region. The sea ice edge is defined as the SIC=15% contour. Monthly mean sea ice concentration data from the Canadian Ice Service are calculated from the beginning or end of each month prior to 2005 and from four weekly data points within a given month thereafter.

3.2 Length of ice season

We define the length of the ice season in the Labrador Sea and Baffin Bay as the number of days when sea ice is present in the region. To this end, we interpolate linearly between the two monthly-mean SIE before and after the (dis-)appearance of sea ice to obtain a Julian day estimate. The error for a given year and location associated with the simple linear interpolation is approximately 1 month (two weeks on either side of the ice season), with much smaller errors when average temporally and spatially due to error cancellation.

We define the length of the ice season for the coastal communities of Nunatsiavut as the number of days when sea ice can be used for subsistence or recreational activities, i.e. a minimum sea ice thickness of 30 cm for the start of the ice season and surface melt onset for the end. The CESM1.3-HR however does not include landfast sea ice parameterizations (e.g. Lemieux et al. 2015) nor does it resolve the fjords along the coastline where a landlock sea ice can developed even in the absence of landfast ice parameterizations. For this reason, we develop a simple predictor for the onset of the sea ice season based on the number freezing degree days (FDD - calculated from ERA5 reanalysis surface air temperature data), starting when satellites first detect ice presence in the fjord (as per weekly Canadian Ice Service ice charts). The end of the sea ice season is set as the first thawing degree days again from ERA5. The model is validated against in-situ sea ice thickness measurements made by the community in Nain from 2009 to 2023 (Nunatsiavut Research Center, 2024).

To this end, we consider a simple 0D, steady state (linear temperature profiles) sea ice thermodynamic model where the conductive heat flux through the ice (F_c^i) and snow (F_c^s) layers are equal and given by (Figure 3.1):

$$F_c^i = -K_i \frac{T_i - T_0}{h_i} = -K_s \frac{T_s - T_i}{h_s} = F_c^s, \tag{3.1}$$

where K_i and K_s are the thermal conductivity of snow (= 0.2 $W/m \cdot K$) and ice (= 2.0 $W/m \cdot K$), T_s, T_i and T_f are the surface, snow-ice interface and freezing point (= 0 $^{\circ}C$) temperatures, and h_i and h_s are the ice thickness (prognostic) and snow depth (assumed constant = 5 cm).

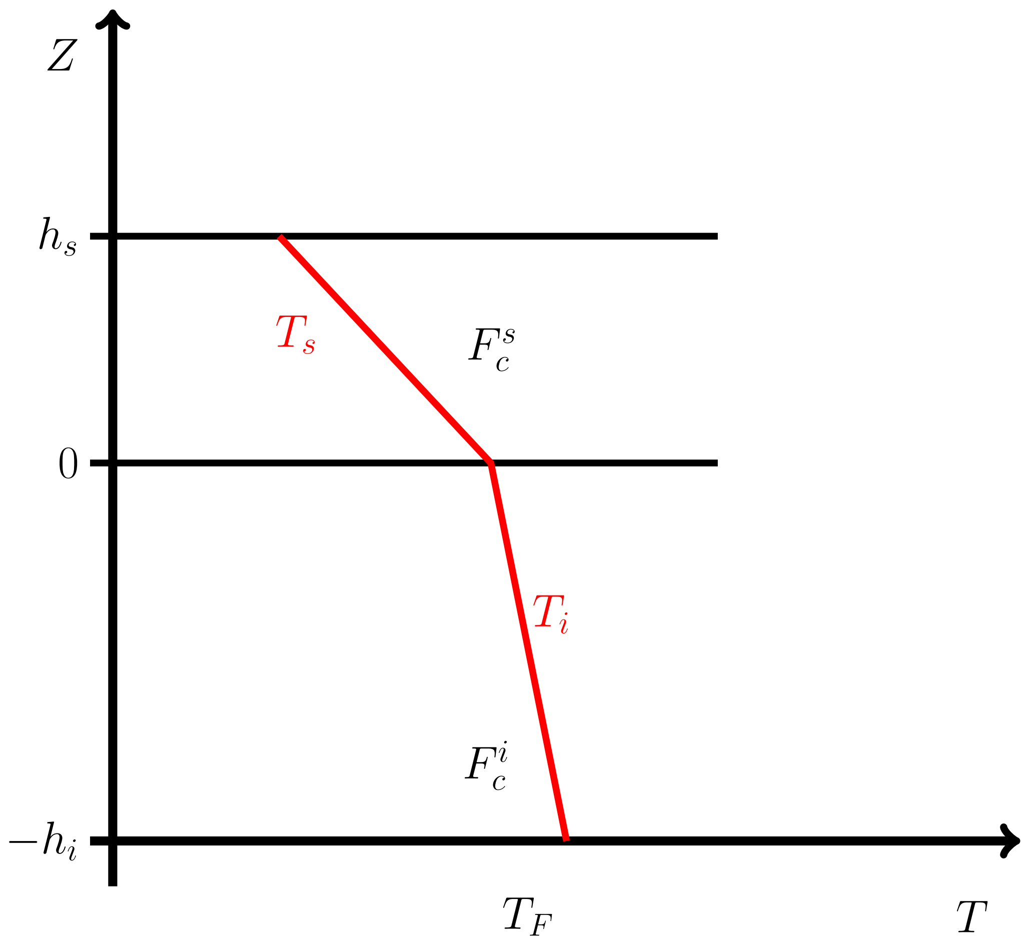

Figure 3.1: Schematic representation of the linear temperature profiles in a 0D steady-state sea ice thermodynamic model, showing the conductive heat flux through the ice (F_c^i) and snow (F_c^s) layers.

Solving for T_i and substituting into F_c^i or F_c^s, we get:

$$F_c = -\frac{K_i K_s}{K_i h_s + K_s h_i} T_s. \tag{3.2}$$

The temporal evolution of the sea ice thickness can then be written as

$$\rho_{Lf}\frac{dh}{dt} = -\frac{K_iK_s}{K_ih_s + K_sh_i}T_s \tag{3.3}$$

Direct integration from t $(= 0$, ice onset) to t and from $h = 0$ m to $h(t)$ yields

$$h = \frac{-K_ih_s \pm \sqrt{(K_ih_s)^2 - 4K_s\frac{K_iK_s\mathrm{FDD}}{\rho_{Lf}}}}{2K_s}, \tag{3.4}$$

where FDD ($= T_st - {}^\circ C \cdot day)$, ρ_i is the ice density $(= 917kg/m^3)$, and L_f is the latent heat of fusion $(= 3.35 \times 10^5 J/kg)$.

Chapter 4

RESULT AND DISCUSSION

4.1 Historical

4.1.1 Seasonality

The simulated seasonality in sea ice extent and trend from pre- to post-2000 is in general agreement with the CIS observation with an onset and disappearance of sea ice in November and August (respectively) and a decline in maximum sea ice extent of $\sim$0.1 million km^2. The maximum sea ice extent and concentration occur primarily due to thermodynamic processes, as opposed to advection of sea ice from the north (see also, Close et al. 2018). Apparent biases in the model include a phase shift of 0.5 month in the seasonality and a negative bias in maximum SIE of $\sim$0.1 million km^2 with less extensive sea ice offshore of Newfoundland and the northern part of the Labrador Sea. The phase shift is associated with an earlier onset of sea ice formation in the northern Baffin Bay and subsequent southward advection, and an earlier decrease in sea ice concentration along the Labrador Coast and southern Baffin Bay starting in April (Mensah et al., 2023; Jordan and

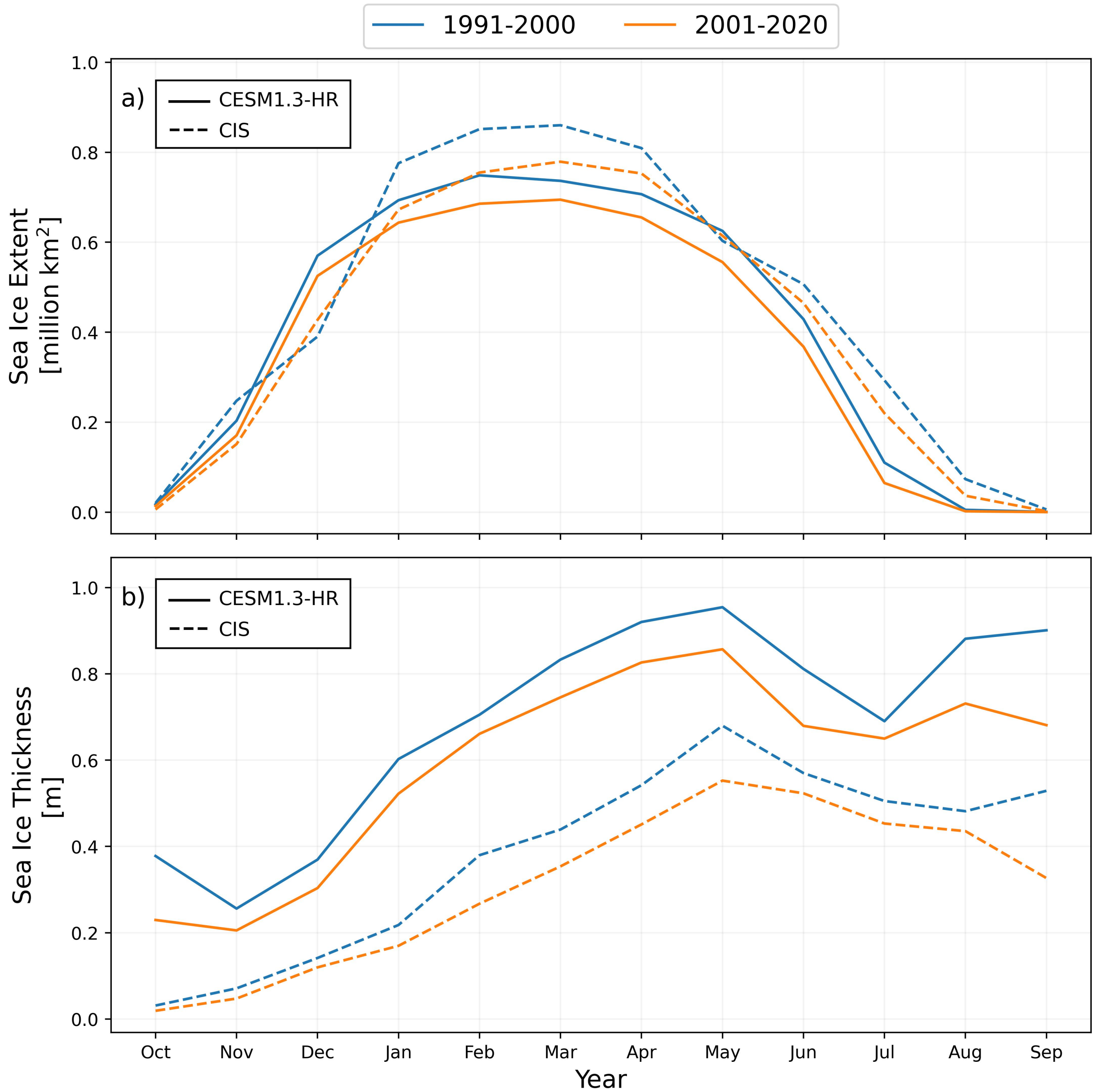

Figure 4.1: (a) Observed (CIS, dashed) and simulated (CESM1.3-HR, solid) monthly mean sea ice extent (SIE) and (b) thickness (SIT) for the 1991-2000 and 2001-2020 time period.

Neu, 1982; Kwok, 2007). The negative bias is in part due to deeper penetration of warm waters by the West Greenland Current (Figure 4.1, 4.2).

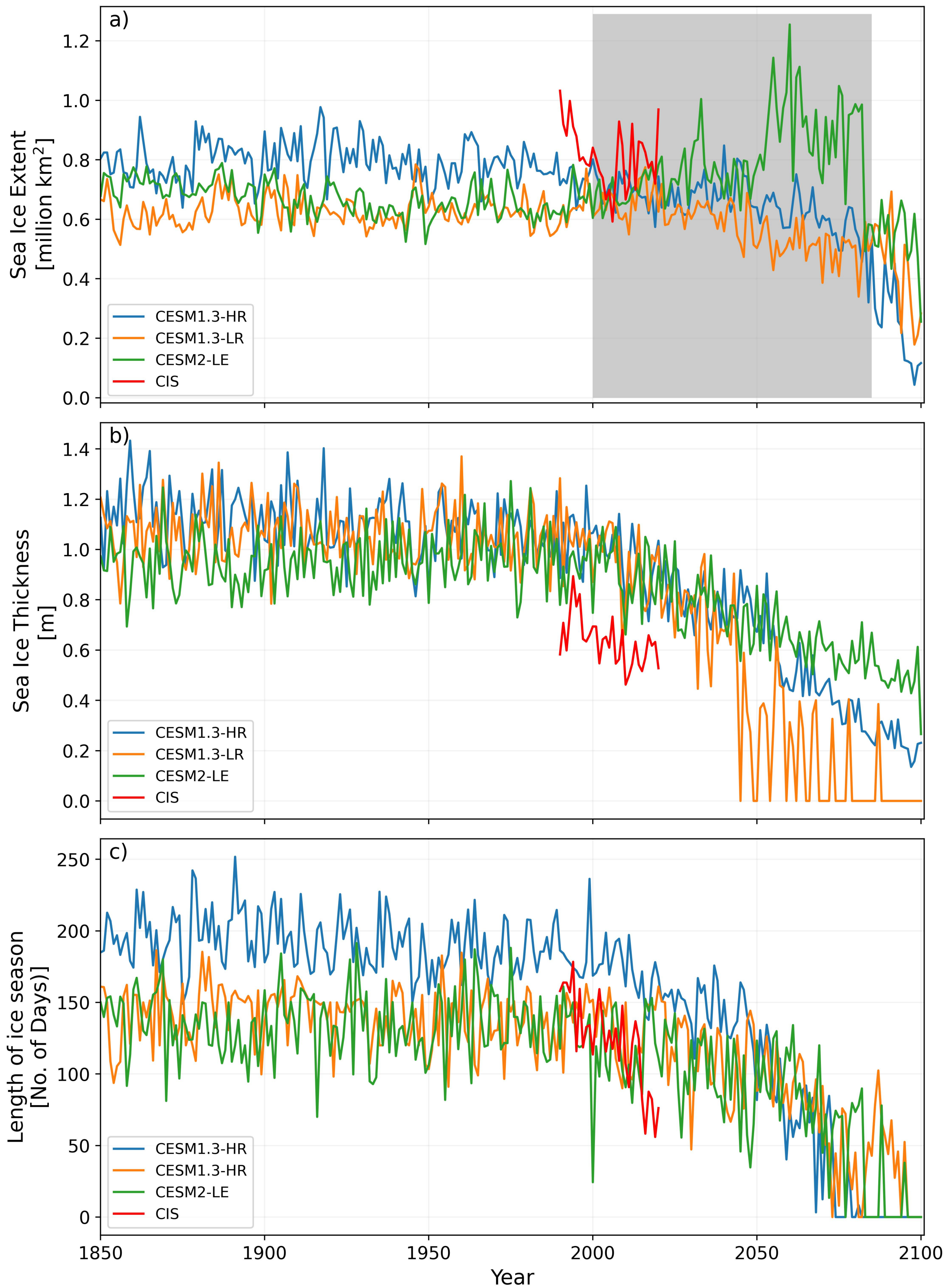

Figure 4.2: Time series of observed (CIS, red) and simulated (CESM2-LE, orange; CESM1.3-HR, blue) (a) March SIE, (b) May SIT and (c)length of ice season from 1850 to 2100.

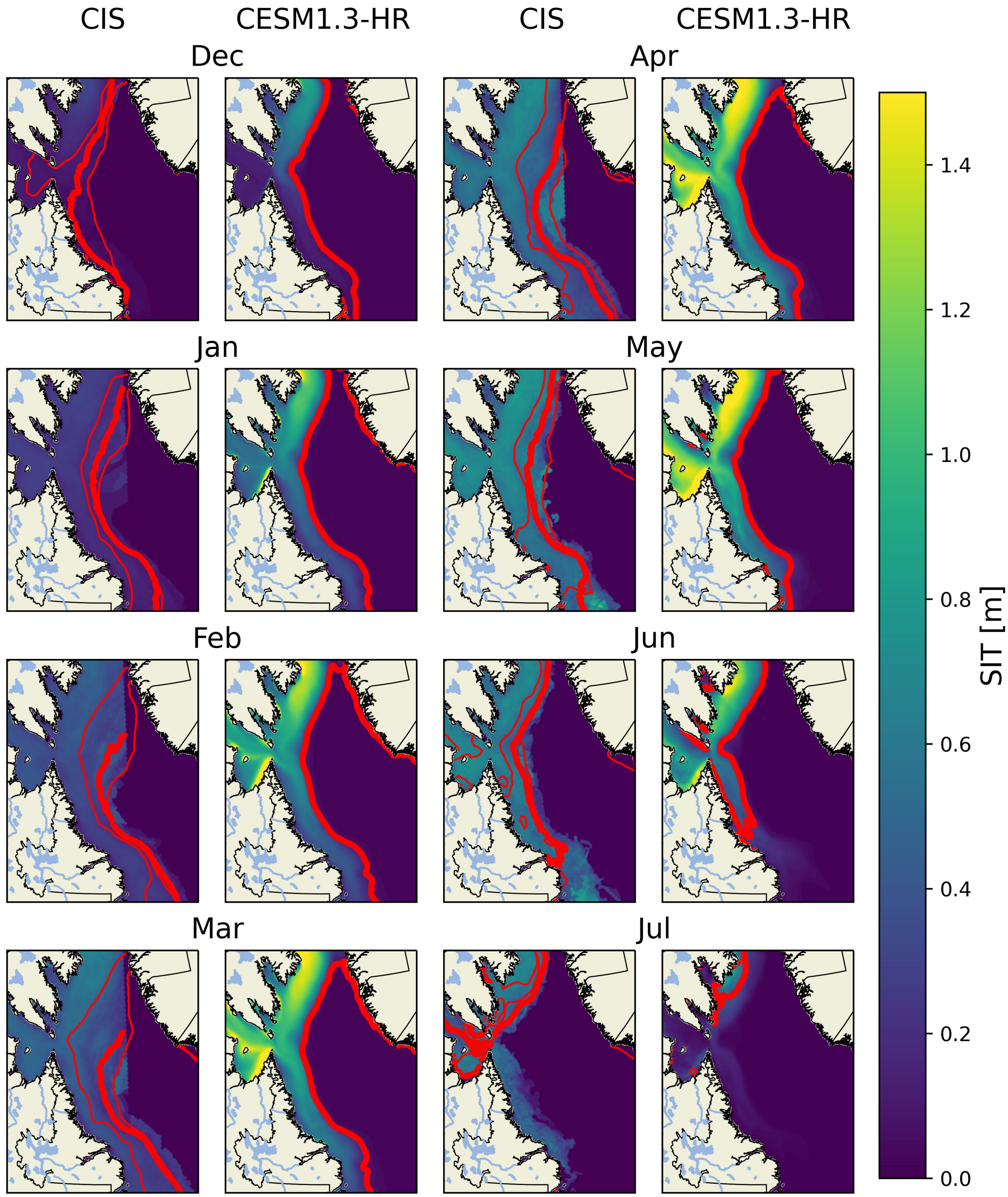

Figure 4.3: Observed (CIS, Column 1 and 3) and Simulated (CESM1.3-HR, Column 2 and 4) spatial distribution of monthly mean SIT for the 1990 - 2020 time period. The bold red contour represents the sea ice edge (SIC=15%), while the thin red contour represents the maximum and minimum SIE from CDR. The thin red contour from CDR is used instead of CIS because CIS and CDR agree with one another (results not shown).

The overestimation of sea ice extent in early winter is attributed to a positive bias in growth rates and the explicit parameterization of vertical ocean heat transport by mesoscale eddies (Chang et al., 2020). Finally, the simulated interannual variability in sea ice edge position is much smaller when compared with observations where large excursions from the mean are sometimes present (see Figure 4.3).

The simulated trend and seasonality in sea ice thickness from pre- to post-2000 follows that of the CIS sea ice thickness proxy with a decrease of $\sim$10 cm from pre- to post-2000, peak in May (0.9 m vs 0.6 m) followed by a decline and a recovery at the end of the melt season. The secondary peak at the end of the summer season is associated with thick multi-year ice in the northern part of the domain that survived the summer melt period (Landy et al., 2017). An exact comparison between CESM1.3-HR and the CIS ice thickness proxy is not possible given that the proxy is derived from partial concentrations of different ice type and stage of development, and not actual sea ice thickness.

4.2 Projections

4.2.1 SIE, SIT and length of ice-free season

The mean and inter-annual variability of the maximum sea ice extent, sea ice thickness and length of ice-free season are in general agreement with observations, except for the simulated SIE that shows smaller magnitudes (Figure 4.2). Projections from CESM1.3-HR show a remarkable stability of the maximum (march) sea ice extent until late in the 21st century (2080) and a more gradual decline in sea ice thickness and length of ice-free season starting in the early 20th century (Figure 4.2, 4.4). The stability in the maximum sea ice extent is due to southward sea-ice advection from northern Baffin Bay and the Lincold Sea; conversely, the rapid decline at the end of the 21st century occurs when this source region of thicker multi-year sea ice disappears eliminating advection of sea ice southward through the Nares Strait and along the Labrador coastline.

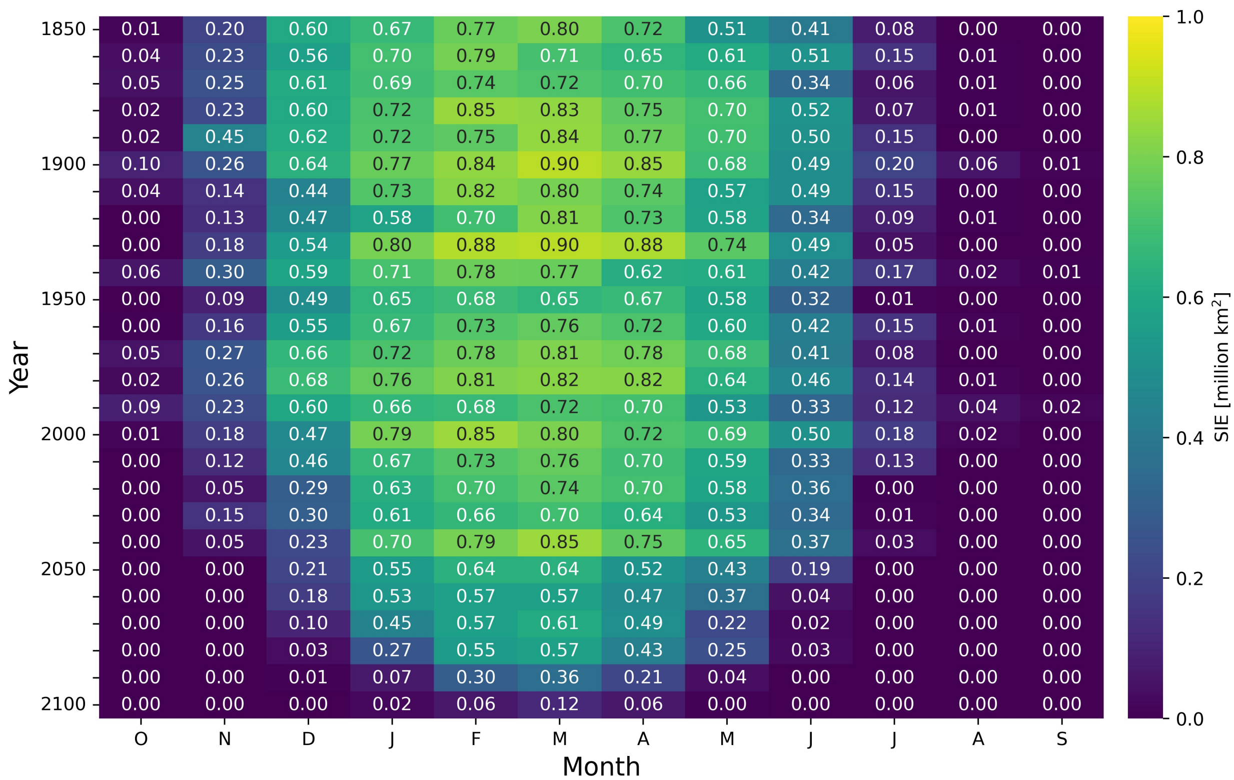

Figure 4.4: Heat map of simulated (CESM1.3-HR) monthly mean SIE for the period of 1850 to 2100.

In the coarser resolution CESM2-LE, the sea ice extent increase in the mid- 21st century, reaching a maximum at the end of the century, followed by a free-fall to ice-free conditions at the end of the century. This difference in behaviour is related to the fate of freshwater from sea ice melt in the Labrador Current – and to a much lesser extent from Greenland ice sheet – that remains trapped in a coastal current in the high resolution model but mixes offshore in the coarser resolution model (Figure 4.2,4.5). The consequence of this

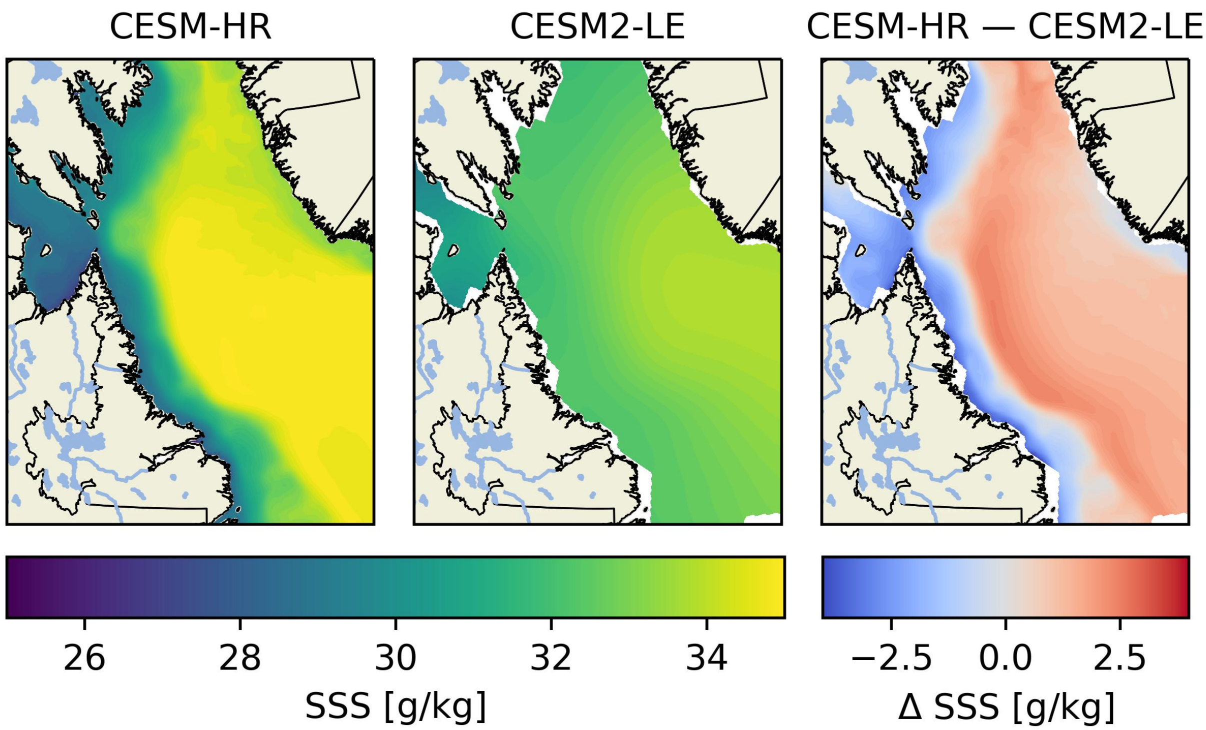

Figure 4.5: Spatial distribution of March sea surface salinity (SSS) for the period of 2060 to 2070 from high (left, CESM1.3-HR) and low-(center, CESM2-LE) resolution models, and the difference between CESM1.3-HR and CESM2-LE (right).

is an increase in stratification, an absence of deep water formation and more favorable conditions for sea ice formation. This change in behaviour as spatial resolution increases was also noted in regional coupled ice-ocean model experiments (e.g, Gou et al. 2022; Dukhovskoy et al. 2019). This shows the importance of resolving fine-scale processes in climate models for regional climate projections.

While the maximum sea ice extent remains stable for the next several decades, the decline in the mean sea ice thickness and length of ice-free season is more gradual starting from ~1 m and 175 days at the beginning of the 21st century and gradually reaching 0.5 m and 75 days when the sharp decline in maximum sea ice extent starts.

4.2.2 Length of ice season in coastal community

The predicted sea ice thickness from the simple 0D thermodynamic model based on FDD is in remarkable agreement (± 10 m) with observed sea ice thickness from Nain giving us confidence in its use to predict the length of the sea ice season for coastal communities using the simulated surface air temperature data from CESM1.3-HR, CESM1.3-LR and CESM2-LE (Figure 4.6). The CIS ice charts suggest the need for ~240 $^{\circ}C \cdot day$ (± 80 $^{\circ}C \cdot day$) for sea ice to first appear in Nain and an additional 200 $^{\circ}C \cdot day$ (or 25 cm) for the establishment of a sea ice cover of 30 cm (Figure 4.6 and 4.7).

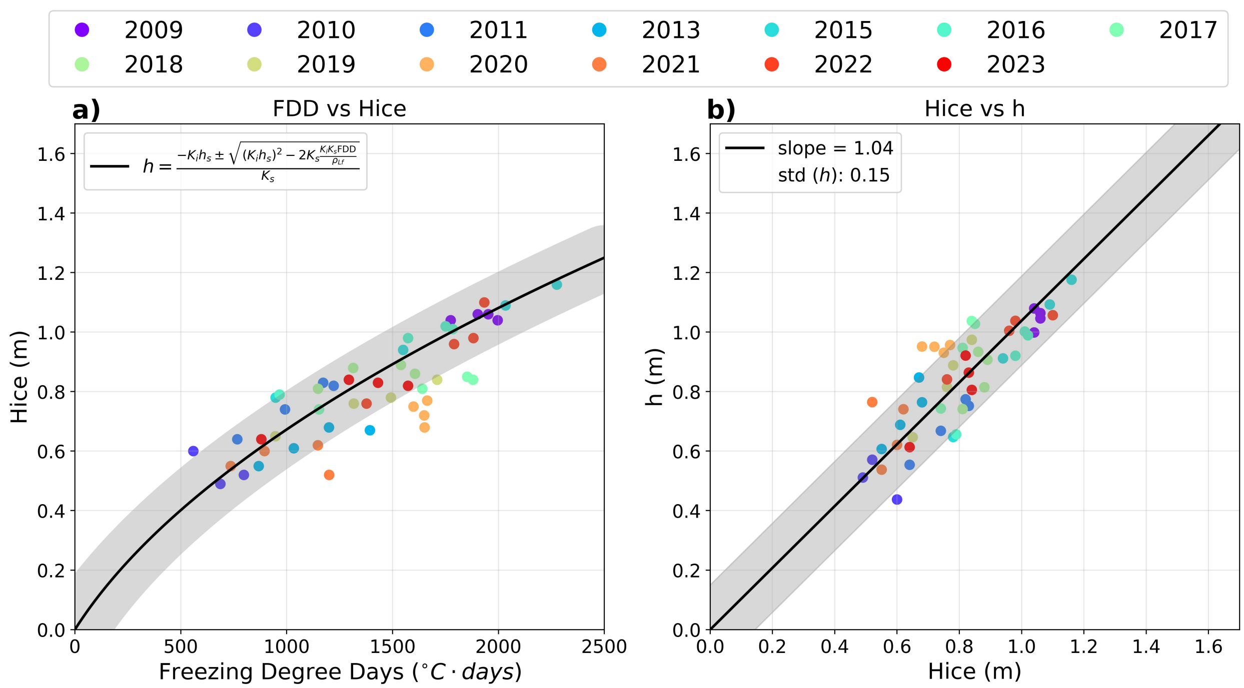

Figure 4.6: (a) In-situ sea ice thickness (Hice) measurements made by the Nunatsiavut Research Center as a function of Freezing Degree Days (FDD) for the period of 2009-2023. The black line and gray shading show the analytical solution (Equation 3.4) derived from FDD and the error bar considering the uncertainty of 7 days on the onset of sea ice formation. (b) Scatter plot of observed (Hice) and FDD-derived (hice) ice thickness. The best line fit forced to pass through the origin has a slope of 1.04 with a standard deviation of 15 cm.

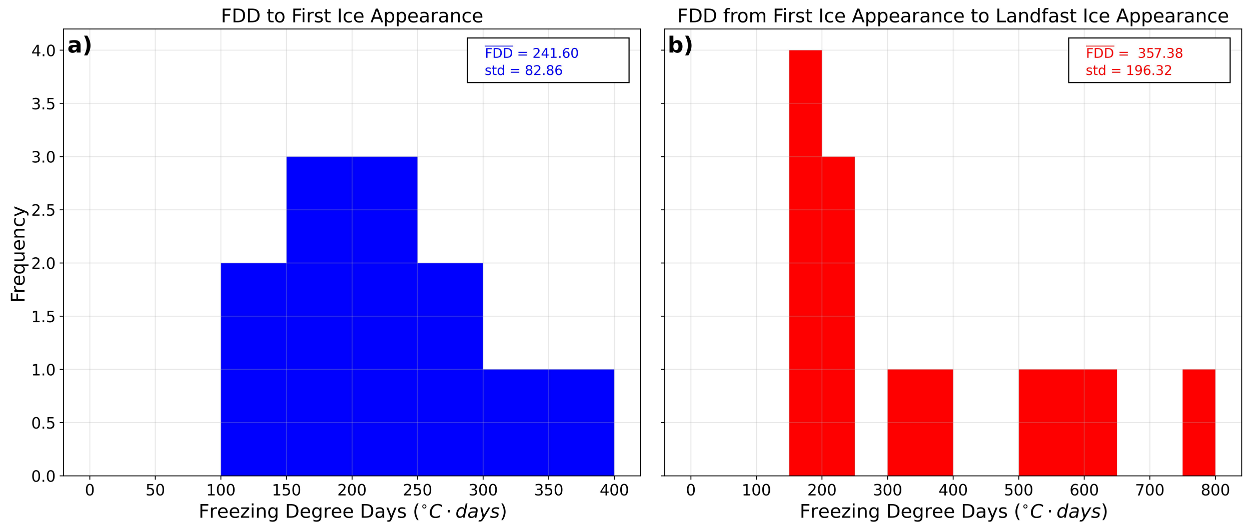

Figure 4.7: Histogram of the distribution of Freezing Degree Days (FDD) prior to the first appearance of ice in Nain as per CIS analyst ($\overline{FDD}$ = 241.60, std = 82.86) and FDD from the first ice appearance to the establishment of a stable landfast ice, with a mean ($\overline{FDD}$ = 357.38, std = 196.32).

The length of the ice season in all four Nnunatsiavut coastal communities (Nain, Hopedale, Postville, and Rigolet) start to decline in the early 20th century from ∼150 days to ∼50-70 days at the end of the 21st century, with a relatively small latitudinal dependence (Figure 4.8). This signal is robust between high and low resolution climate models. In all four locations, inter-annual varaibility in the length of the ice season increases in the 21st century from ∼50 to ∼100 with sporadic extremely large variability reaching 200 days.

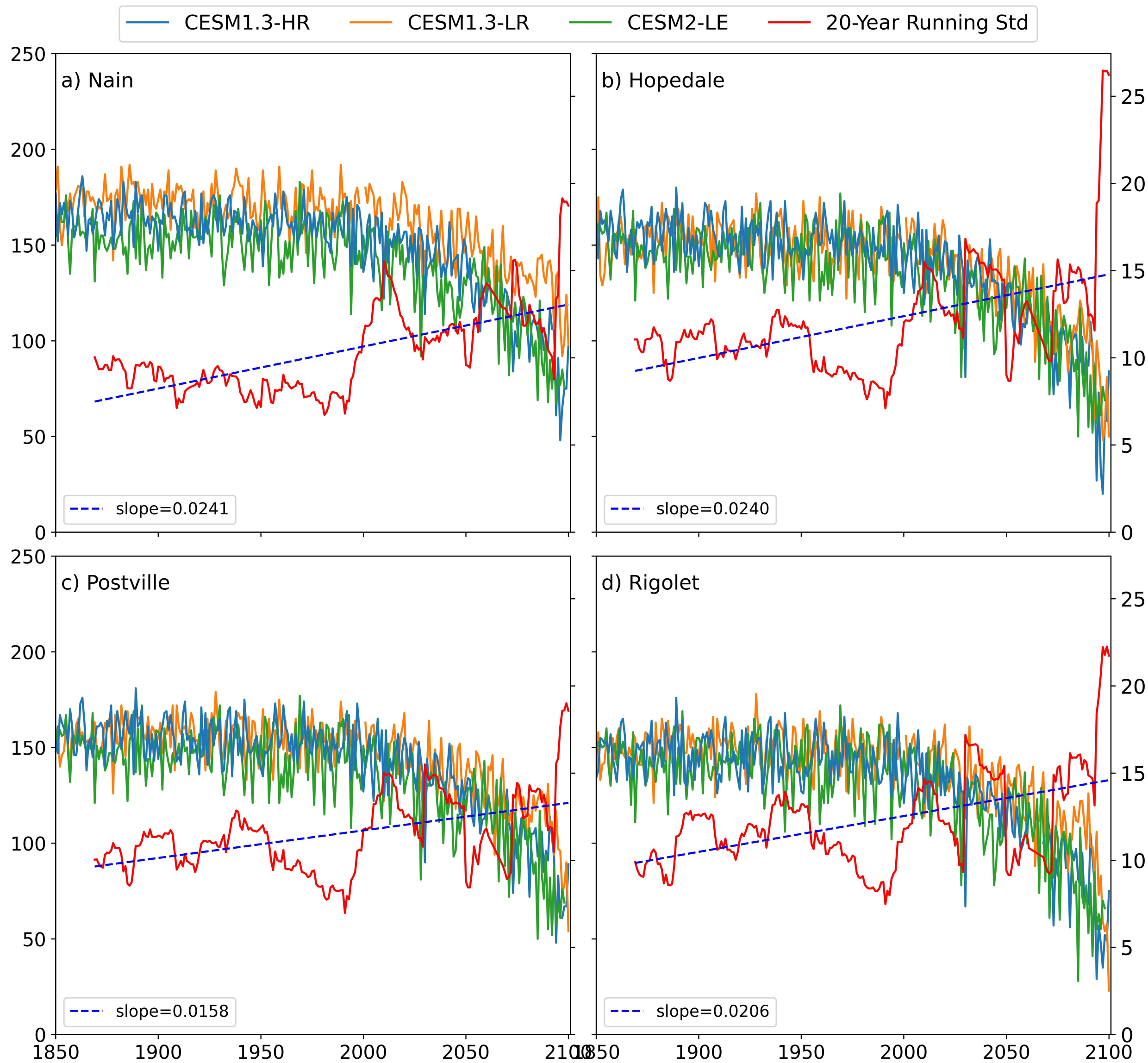

Figure 4.8: Time series of the length of the ice season (number of days) and 20-year running standard deviation (red) for four locations in Labrador: (a) Nain, (b) Hopedale, (c) Postville, and (d) Rigolet. The data compares simulations from three different models: CESM1.3-HR (blue), CESM1.3-LR (orange), and CESM2-LE (green), with slope (Blue dashed), covering the period from 1850 to 2100.

Chapter 5

CONCLUSION AND FUTURE WORK

Sea ice serves as the primary highway for the people of Nunatsiavut, bridging both the tangible aspects of transportation and the intangible cultural connections to the land and sea. In this study, we present projections of ice season length for coastal communities of Nunatsiavut from both low- and high-resolution Community Earth System Models, namely the CESM1.3-HR, CESM1.3-LR, and CESM2-LE.

Results show that the maximum March sea ice extent remains remarkably stable until approximately 2060, after which a rapid transition to ice-free conditions occurs by the end of the century. This stability is attributed to the continued southward advection of sea ice from the northern Baffin Bay and Lincoln Sea.

In contrast, projections from the coarser resolution CESM2-LE model show an increase in sea ice extent starting in the mid- 21st century, followed by a sudden collapse. The difference in behaviour is linked with the fate of freshwater from sea ice melt in the coastal Labrador Current that mixes laterally in the low resolution model, shuts down convection, leading to a re-expansion of the maximum sea ice extent. In the high-resolution model, instead, freshwater remains coastally trapped, and deep convection remains active during the transition to an ice-free Arctic. This difference in behaviour highlights the importance of high-resolution modeling in capturing fine-scale processes essential for accurate regional climate projections.

Given that landfast ice and fjords along the Labrador coastlines are not resolved in the low- and high-resolution models, changes in the length of the ice season is estimated from a simple ice-thickness – freezing degree day (FDD) relationship derived from in-situ ice thickness measurements from Nain and Canadian Ice charts for onset of the ice season. Results also show a gradual decline in sea ice thickness and the length of the ice season starting early in the 21st century with sporadic large ice increase in inter-annual variability. This decline begins from an initial mean thickness of 1 meter and a season length of 175 days, gradually decreasing to 0.5 meters and 75 days before the sharp decline in maximum sea ice extent occurs. This reduction is associated with later freeze-up (60%) and earlier breakup (40%) of sea ice, driven by increasing air and sea temperatures.

Landfast ice parameterizations are currently being included as default in the Community Sea Ice code (CICE). This will allow for a direct assessment of changes in the length of the ice season and comparison of the simple FDD and simulated ice thickness fields using a consistent simulated data sets from the Community Earth System model.

Bibliography

ACIA (2004). *Impacts of a Warming Climate: Arctic Climate Impact Assessment*. Cambridge University Press, Cambridge.

Agnew, T. and Howell, S. (2003). The use of operational ice charts for evaluating passive microwave ice concentration data. *Atmosphere-ocean*, 41(4):317–331.

Bailey, D., Holland, M., Hunke, E., Lipscomb, B., Briegleb, B., Bitz, C., and Schramm, J. (2011). Community ice code (cice) user's guide version 4.0 released with ccsm 4.0. Technical report, Los Alamos National Laboratory, Los Alamos, New Mexico.

Bitz, Holland, Weaver, A., and Eby, M. (2001). Simulating the ice-thickness distribution in a coupled climate model. *Journal of Geophysical Research*, 106:2441–2463.

Bitz and Lipscomb, W. H. (1999). An energy-conserving thermodynamic model of sea ice. *Journal of Geophysical Research: Oceans*, 104(C7):15669–15677.

Cavalieri, D., Parkinson, C., Gloersen, P., and Zwally, H. (1997). Arctic and antarctic sea ice concentrations from multichannel passive-microwave satellite data sets: October 1978–september 1995. *User's Guide NASA Technical Memorandum*, 104647:1–17. NASA Goddard Space Flight Center, Greenbelt, MD.

Cavalieri, D. J., Gloersen, P., and Campbell, W. J. (1984). Determination of sea ice parameters with the nimbus 7 smmr. *Journal of Geophysical Research: Atmospheres*, 89(D4):5355–5369.

CBC News (2021). The sea ice in northern labrador is thinning — fast. here's why the inuit are worried. `https://www.cbc.ca/news/canada/newfoundland-labrador/labrador-nunatsiavut-sea-ice-1.5951551`.

CESM2 (2020). Community earth system model project configurations. Accessed: 2023-07-15.

CESM2-LE (2023). Community earth system model project large ensemble phase 2. Accessed: July 2023.

Chang, P., Zhang, S., Danabasoglu, G., Yeager, S. G., Fu, H., Wang, H., Castruccio, F. S., Chen, Y., Edwards, J., Fu, D., et al. (2020). An unprecedented set of high-resolution earth system simulations for understanding multiscale interactions in climate variability and change. *Journal of Advances in Modeling Earth Systems*, 12(12):e2020MS002298.

Close, S., Herbaut, C., Houssais, M.-N., and Blaizot, A.-C. (2018). Mechanisms of interannual-to decadal-scale winter labrador sea ice variability. *Climate dynamics*, 51(7):2485–2508.

Comiso (2023). Bootstrap sea ice concentrations from nimbus-7 smmr and dmsp ssm/i-ssmis, version 4.

Comiso, J. (1995). Ssm/i concentrations using the bootstrap algorithm, nasa reference publication 1380.

Comiso, J. C. (1986). Characteristics of arctic winter sea ice from satellite multispectral microwave observations. *Journal of Geophysical Research: Oceans*, 91(C1):975–994.

Comiso, J. C. and Nishio, F. (2008). Trends in the sea ice cover using enhanced and compatible amsr-e, ssm/i, and smmr data. *Journal of Geophysical Research: Oceans*, 113(C2).

Cuerrier, A., Brunet, N. D., Gérin-Lajoie, J., Downing, A., and Lévesque, E. (2015). The study of inuit knowledge of climate change in nunavik, quebec: a mixed methods approach. *Human ecology*, 43:379–394.

Cunsolo, A., Shiwak, I., Wood, M., and Team, I.-I. (2017). "you need to be a well-rounded cultural person": youth mentorship programs for cultural preservation, promotion, and sustainability in the nunatsiavut region of labrador. *Northern sustainabilities: understanding and addressing change in the circumpolar world*, pages 285–303.

Danabasoglu, G., Yeager, S. G., Kwon, Y.-O., Tribbia, J. J., Phillips, A. S., and Hurrell, J. W. (2012). Variability of the atlantic meridional overturning circulation in ccsm4. *Journal of climate*, 25(15):5153–5172.

Deser, C., Holland, M., Reverdin, G., and Timlin, M. (2002). Decadal variations in labrador sea ice cover and north atlantic sea surface temperatures. *Journal of Geophysical Research: Oceans*, 107(C5):3–1.

Deser, C., Magnusdottir, G., Saravanan, R., and Phillips, A. (2004). The effects of north atlantic sst and sea ice anomalies on the winter circulation in ccm3. part ii: Direct and indirect components of the response. *Journal of Climate*, 17(5):877–889.

Dukhovskoy, D., Yashayaev, I., Proshutinsky, A., Bamber, J., Bashmachnikov, I., Chassignet, E., Lee, C., and Tedstone, A. (2019). Role of greenland freshwater anomaly in the recent freshening of the subpolar north atlantic. *Journal of Geophysical Research: Oceans*, 124(5):3333–3360.

Eden, C. and Willebrand, J. (2001). Mechanism of interannual to decadal variability of the north atlantic circulation. *Journal of Climate*, 14(10):2266–2280.

Eyring, V., Bony, S., Meehl, G. A., Senior, C. A., Stevens, B., Stouffer, R. J., and Taylor, K. E. (2016). Overview of the coupled model intercomparison project phase 6 (cmip6) experimental design and organization. *Geoscientific Model Development*, 9(5):1937–1958.

Felt, L., Procter, A. H., and Natcher, D. C. (2012). *Settlement, subsistence, and change among the Labrador Inuit: The Nunatsiavummiut experience*, volume 2. Univ. of Manitoba Press.

Galley, R. J., Else, B. G., Howell, S. E., Lukovich, J. V., and Barber, D. G. (2012). Landfast sea ice conditions in the canadian arctic: 1983-2009. *Arctic*, pages 133–144.

Gearheard, S., Matumeak, W., Angutikjuaq, I., Maslanik, J., Huntington, H. P., Leavitt, J., Kagak, D. M., Tigullaraq, G., and Barry, R. G. (2006). "it's not that simple": a collaborative comparison of sea ice environments, their uses, observed changes, and adaptations in barrow, alaska, usa, and clyde river, nunavut, canada. *AMBIO: A Journal of the Human Environment*, 35(4):203–211.

Gou, R., Pennelly, C., and Myers, P. G. (2022). The changing behavior of the west greenland current system in a very high-resolution model. *Journal of Geophysical Research: Oceans*, 127(8):e2022JC018404.

Häkkinen, S. (2002). Surface salinity variability in the northern north atlantic during recent decades. *Journal of Geophysical Research: Oceans*, 107(C12):SRF–4.

Han, G., Ma, Z., Long, Z., Perrie, W., and Chassé, J. (2019). Climate change on newfoundland and labrador shelves: Results from a regional downscaled ocean and sea-ice model under an a1b forcing scenario 2011–2069. *Atmosphere-Ocean*, 57(1):3–17.

Hersbach, H., Bell, B., Berrisford, P., Biavati, G., Horányi, A., Muñoz Sabater, J., Nicolas, J., Peubey, C., Radu, R., Rozum, I., Schepers, D., Simmons, A., Soci, C., Dee, D., and Thépaut, J.-N. (2023). Era5 hourly data on single levels from 1940 to present. Accessed on 26-Jun-2026.

Heyblom, K. B., Singh, H. A., Rasch, P. J., and DeRepentigny, P. (2022). Increased variability of biomass burning emissions in cmip6 amplifies hydrologic cycle in the cesm2 large ensemble. *Geophysical Research Letters*, 49(5):e2021GL096868.

Howell, S., Babb, D., Landy, J. C., Moore, G., Montpetit, B., and Brady, M. (2023). A comparison of arctic ocean sea ice export between nares strait and the canadian arctic archipelago. *Journal of Geophysical Research: Oceans*, 128(4):e2023JC019687.

Hunke, E. and Dukowicz, J. (2002). The elastic viscous plastic sea ice dynamics model in general orthogonal curvilinear coordinates on a sphere—incorporation of metric terms. *Monthly Weather Review - MON WEATHER REV*, 130.

Hunke, E., Lipscomb, W., Jones, P., Turner, A., Jeffery, N., and Elliott, S. (2017). Cice, the los alamos sea ice model, version 00. *URL: https://www. osti. gov/biblio/1364126*.

Hunke, E., Lipscomb, W. H., Turner, A. K., Jeffery, N., and Elliott, S. (2010). Cice: the los alamos sea ice model documentation and software user's manual version 4.1 la-cc-06-012. *T-3 Fluid Dynamics Group, Los Alamos National Laboratory*, 675:500.

JCOMM (2004). SIGRID 3: A Vector Archive Format for Sea Ice Charts. Technical Report 23, Joint WMO-IOC Technical Commission for Oceanography and Marine Meteorology, Geneva, Switzerland.

Jordan, F. and Neu, H. (1982). Ice drift in southern baffin bay and davis strait: Research note. *Atmosphere-Ocean*, 20(3):268–275.

Kern, S., Lavergne, T., Notz, D., Pedersen, L. T., and Tonboe, R. (2020). Satellite passive microwave sea-ice concentration data set inter-comparison for arctic summer conditions. *The Cryosphere*, 14(7):2469–2493.

Kwok, R. (2005). Variability of nares strait ice flux. *Geophysical Research Letters*, 32(24).

Kwok, R. (2007). Baffin bay ice drift and export: 2002–2007. *Geophysical Research Letters*, 34(19).

Landy, J. C., Ehn, J. K., Babb, D. G., Thériault, N., and Barber, D. G. (2017). Sea ice thickness in the eastern canadian arctic: Hudson bay complex & baffin bay. *Remote Sensing of Environment*, 200:281–294.

Large, W. G., McWilliams, J. C., and Doney, S. C. (1994). Oceanic vertical mixing: A review and a model with a nonlocal boundary layer parameterization. *Reviews of Geophysics*, 32(4):363–403.

Lawrence, D. M., Oleson, K. W., Flanner, M. G., Thornton, P. E., Swenson, S. C., Lawrence, P. J., Zeng, X., Yang, Z.-L., Levis, S., Sakaguchi, K., et al. (2011). Parameterization improvements and functional and structural advances in version 4 of the community land model. *Journal of Advances in Modeling Earth Systems*, 3(1).

Lemieux, J.-F., Tremblay, L. B., Dupont, F., Plante, M., Smith, G. C., and Dumont, D. (2015). A basal stress parameterization for modeling landfast ice. *Journal of Geophysical Research: Oceans*, 120(4):3157–3173.

Lipscomb, W. H. (2001). Remapping the thickness distribution in sea ice models. *Journal of Geophysical Research: Oceans*, 106(C7):13989–14000.

Mahoney, A., Gearheard, S., Oshima, T., and Qillaq, T. (2009). Sea ice thickness measurements from a community-based observing network. *Bulletin of the American Meteorological Society*, 90(3):370–378.

Meehl, G. A., Yang, D., Arblaster, J. M., Bates, S. C., Rosenbloom, N., Neale, R., Bacmeister, J., Lauritzen, P. H., Bryan, F., Small, J., et al. (2019). Effects of model resolution, physics, and coupling on southern hemisphere storm tracks in cesm1. 3. *Geophysical Research Letters*, 46(21):12408–12416.

Meier, Fetterer, Windnagel, and Stewart (2021). Noaa/nsidc climate data record of passive microwave sea ice concentration, version 4.

Mensah, V., Fujita, K., Howell, S., Ikeda, M., Komatsu, M., and Ohshima, K. I. (2023). Estimation of ice melt, freshwater budget, and their multi-decadal trends in the baffin bay and labrador sea. *EGUsphere*, 2023:1–33.

Münchow, A. (2016). Volume and freshwater flux observations from nares strait to the west of greenland at daily time scales from 2003 to 2009. *Journal of Physical Oceanography*, 46(1):141–157.

Muntjewerf, L., Sacks, W. J., Lofverstrom, M., Fyke, J., Lipscomb, W. H., Ernani da Silva, C., Vizcaino, M., Thayer-Calder, K., Lenaerts, J. T., and Sellevold, R. (2021). Description and demonstration of the coupled community earth system model v2–community ice sheet model v2 (cesm2-cism2). *Journal of Advances in Modeling Earth Systems*, 13(6):e2020MS002356.

Neale, R. B., Chen, C.-C., Gettelman, A., Lauritzen, P. H., Park, S., Williamson, D. L., Conley, A. J., Garcia, R., Kinnison, D., Lamarque, J.-F., et al. (2010). Description of the ncar community atmosphere model (cam 5.0). *NCAR Tech. Note NCAR/TN-486+ STR*, 1(1):1–12.

Newswire (2021). Canada invests in inuit-led climate adaptation and conservation in nunatsiavut, newfoundland and labrador. https://www.newswire.ca/news-releases/canada-invests-in-inuit-led-climate-adaptation-and-conservation-in-nunatsiavut-newfoundland-and-labrador-809891914.html.

Nickels, S., Furgal, C., Buell, M., Moquin, H., et al. (2005). *Unikkaaqatigiit: Putting the human face on climate change-Perspectives from Inuit in Canada*. Joint publication of Inuit Tapiriit Kanatami, Nasivvik Centre for Inuit ....

Notz, D. and Community, S. (2020). Arctic sea ice in cmip6. *Geophysical Research Letters*, 47(10):e2019GL086749.

Nunatsiavut Research Center (2024). Ice thickness data from nain, nunatsiavut (2009-2023). Unpublished raw data. Accessed February 2024.

Olauson, J. (2018). Era5: The new champion of wind power modelling? *Renewable energy*, 126:322–331.

Ouellet-Bernier, M.-M., de Vernal, A., Chartier, D., and Boucher, É. (2021a). Historical perspectives on exceptional climatic years at the labrador/nunatsiavut coast 1780 to 1950. *Quaternary Research*, 101:114–128.

Ouellet-Bernier, M.-M., de Vernal, A., and Sea, L. (2021b). Winter freeze-up and summer break-up in nunatsiavut, canada, from 1770 to 1910. *CONTRIBUTION DES SOURCES HISTORIQUES À L'ÉTUDE DU CLIMAT DE LA CÔTE DU LABRADOR/NUNATSIAVUT, 1750 À 1950: UN REGARD SUR LES SOURCES DISCURSIVES, DOCUMENTAIRES ET INSTRUMENTALES*, page 221.

Pearce, T. D., Ford, J. D., Laidler, G. J., Smit, B., Duerden, F., Allarut, M., Andrachuk, M., Baryluk, S., Dialla, A., Elee, P., et al. (2009). Community collaboration and climate change research in the canadian arctic. *Polar Research*, 28(1):10–27.

Pizzolato, L., Howell, S. E., Derksen, C., Dawson, J., and Copland, L. (2014). Changing sea ice conditions and marine transportation activity in canadian arctic waters between 1990 and 2012. *Climatic change*, 123:161–173.

Rodgers, K. B., Lee, S.-S., Rosenbloom, N., Timmermann, A., Danabasoglu, G., Deser, C., Edwards, J., Kim, J.-E., Simpson, I. R., Stein, K., et al. (2021). Ubiquity of human-induced changes in climate variability. *Earth System Dynamics*, 12(4):1393–1411.

Small, R. J., Bacmeister, J., Bailey, D., Baker, A., Bishop, S., Bryan, F., Caron, J., Dennis, J., Gent, P., Hsu, H.-m., et al. (2014). A new synoptic scale resolving global climate simulation using the community earth system model. *Journal of Advances in Modeling Earth Systems*, 6(4):1065–1094.

Smith, R., Jones, P., Briegleb, B., Bryan, F., Danabasoglu, G., Dennis, J., Dukowicz, J., Eden, C., Fox-Kemper, B., Gent, P., et al. (2010). The parallel ocean program (pop) reference manual ocean component of the community climate system model (ccsm) and community earth system model (cesm). *LAUR-01853*, 141:1–140.

Statistics Canada (2012). Environment: Overview. Accessed: 2024-06-29.

Tivy, A., Howell, S. E., Alt, B., McCourt, S., Chagnon, R., Crocker, G., Carrieres, T., and Yackel, J. J. (2011). Trends and variability in summer sea ice cover in the canadian arctic based on the canadian ice service digital archive, 1960–2008 and 1968–2008. *Journal of Geophysical Research: Oceans*, 116(C3).

Urban, A., Di Napoli, C., Cloke, H. L., Kyselỳ, J., Pappenberger, F., Sera, F., Schneider, R., Vicedo-Cabrera, A. M., Acquaotta, F., Ragettli, M. S., et al. (2021). Evaluation of the era5 reanalysis-based universal thermal climate index on mortality data in europe. *Environmental research*, 198:111227.

Urraca, R., Huld, T., Gracia-Amillo, A., Martinez-de Pison, F. J., Kaspar, F., and Sanz-Garcia, A. (2018). Evaluation of global horizontal irradiance estimates from era5 and cosmo-rea6 reanalyses using ground and satellite-based data. *Solar Energy*, 164:339–354.

Vaideanu, P., Stepanek, C., Dima, M., Schrepfer, J., Matos, F., Ionita, M., and Lohmann, G. (2023). Large-scale sea ice–surface temperature variability linked to atlantic meridional overturning circulation. *Plos one*, 18(8):e0290437.

Van Marle, M. J., Kloster, S., Magi, B. I., Marlon, J. R., Daniau, A.-L., Field, R. D., Arneth, A., Forrest, M., Hantson, S., Kehrwald, N. M., et al. (2017). Historic global biomass burning emissions for cmip6 (bb4cmip) based on merging satellite observations with proxies and fire models (1750–2015). *Geoscientific Model Development*, 10(9):3329–3357.

Weijer, W., Haine, T. W., Siddiqui, A. H., Cheng, W., Veneziani, M., and Kurtakoti, P. (2021). Interactions between the arctic mediterranean and the atlantic meridional overturning circulation: A review. *Oceanography*. Received 23 June 2017, Accepted 21 November 2017, Published 02 December 2017, Issue Date October 2018.

Wu, Y., Zhao, X., Qi, Z., Zhou, K., and Qiao, D. (2023). Relative contribution of atmospheric forcing, oceanic preconditioning and sea ice to deep convection in the labrador sea. *Journal of Marine Science and Engineering*, 11(4):869.

Yashayaev, I. (2024). Intensification and shutdown of deep convection in the labrador sea were caused by changes in atmospheric and freshwater dynamics. *Communications Earth & Environment*, 5:156. Accessed: 2024-06-29.

Yashayaev, I., van Aken, H. M., Holliday, N. P., and Bersch, M. (2007). Transformation of the labrador sea water in the subpolar north atlantic. *Geophysical Research Letters*, 34(22).

Yu, Y., Xiao, W., Zhang, Z., Cheng, X., Hui, F., and Zhao, J. (2021). Evaluation of 2-m air temperature and surface temperature from era5 and era-i using buoy observations in the arctic during 2010–2020. *Remote Sensing*, 13(14):2813.

Zhang, S., Fu, H., Wu, L., Li, Y., Wang, H., Zeng, Y., Duan, X., Wan, W., Wang, L., Zhuang, Y., Meng, H., Xu, K., Xu, P., Gan, L., Liu, Z., Wu, S., Chen, Y., Yu, H., Shi, S., Wang, L., Xu, S., Xue, W., Liu, W., Guo, Q., Zhang, J., Zhu, G., Tu, Y., Edwards, J., Baker, A., Yong, J., Yuan, M., Yu, Y., Zhang, Q., Liu, Z., Li, M., Jia, D., Yang, G., Wei, Z., Pan, J., Chang, P., Danabasoglu, G., Yeager, S., Rosenbloom, N., and Guo, Y. (2020). Optimizing high-resolution community earth system model on a heterogeneous many-core supercomputing platform. *Geoscientific Model Development*, 13(10):4809–4829.

Zhu, J., Xie, A., Qin, X., Wang, Y., Xu, B., and Wang, Y. (2021). An assessment of era5 reanalysis for antarctic near-surface air temperature. *Atmosphere*, 12(2):217.